Mineralogical transformations in the Fe-laterite profiles of Saudi Arabia: A study of weathering dynamics and secondary lateritization

Rami A. Bakhsh [1], Ali A. Mesaed [2, 3, *]

[1]Department of Mineral Resources and Rocks, Faculty of Earth Sciences, King Abdulaziz University, P.O. Box 80206, Jeddah 21589, Saudi Arabia
[2]Geo-Exploration Techniques Department, Faculty of Earth Sciences, King Abdulaziz University, P.O. Box 80206, Jeddah 21589, Saudi Arabia
[3]Geology Department, Faculty of Sciences, Cairo University, Giza, Egypt

A B S T R A C T

This study examines an iron-rich laterite profile, 4 to 9 meters thick, located between the ancient Precambrian Arabian Shield rocks and the younger Phanerozoic layers in Saudi Arabia. The profile begins with hard parent rocks composed of quartz diorite and gabbro containing iron-silicate. As these rocks weather, they become progressively softer and more clay-like, forming slightly and highly weathered argillaceous rocks. The Fe-laterite profile includes three main layers: the original parent rocks, the slightly altered rocks (saprolite), and the highly altered argillaceous rocks at the top. Samples from different layers of the weathering profile were collected and analyzed for their mineral content. The original quartz diorite and gabbro primarily consist of feldspars, hornblende, chlorite, and quartz. In the slightly altered layer, the hornblende and chlorite expand and peel apart, while the feldspar crystals transform into kaolinite and sericite. In the highly altered top layer, the remaining iron-silicate minerals show significant curling and breaking apart, and the surrounding clay becomes more uniform, composed mainly of mixed dark iron-oxyhydroxides and a light aluminum- and silicon-rich gel with small amounts of quartz. The study explores the progressive stages of weathering, including: a) Initial breakdown of iron-silicate minerals through hydrolysis and oxidation, b) Further destruction of these minerals and the formation of goethite, hematite, and kaolinite, c) Final stages where kaolinite and small microcrystalline quartz aggregates form from silica leached from higher layers, a process known as secondary lateritization.

1. Introduction

The chemical weathering of various ferromagnesian minerals and the formation of secondary iron minerals has been examined by many researchers, including Murphy et al. (1998), Dong et al. (1998), Hampl et al. (2023), and Yi et al. (2023). The mechanism of weathering of phyllosilicate minerals in general and biotite and chlorites in particular has been currently studied in detail by Price and Velbel (2014) and Xi et al. (2024). To understand the processes of chemical weathering, a lot of experimental works have been carried out to illustrate the mechanism and steps of the destruction of the different ferromagnesian minerals under systematically variable pH and Eh conditions, e.g., Drever (1971), Berner et al. (1980), Siever and Woodford (1979), Nahon (1987), Grandstaff (1977), Luce et al. (1972), Farmer et al. (1971), Nahon and Colin (1982), Berner and Schott (1982), Meunier and Velde (1979), Walker et al. (1967), He et al. (2023), Kukillaya and Narayanan (2014), and Eswaran (1979). The mode of formation of the weathering profiles and their economic aspects in Egypt were studied by many authors, e.g., El Aref (1993), El-Hinnawi et al. (2021), and Germann et al. (1994), and Mesaed (1995). El Aref (1993) related the formation of Um Gereifate iron ore of the Red Sea Coastal Zone to the lateritic weathering of the underlying granitic rocks. Mesaed (1995) studied in detail the different lateritic products just underlying the Turonian clastics of the Abu Agag Formation, East Aswan area and discussed the currently postulated theory concerning the derivation of

Aswan ironstone (iron ore) by the lateritic weathering of the underlying Precambrian rocks, i.e., quartz biotite schist and hornblende schist. The study aims to shed light on the progressive and subsequent stages of mineral degradation and alteration of the crystalline igneous rocks by chemical weathering processes beginning from the fresh parental rocks until the iron-rich argillaceous soft rocks (Fe-laterite horizon).

2. Methods of the study

The study relies primarily on detailed and systematic field observations, measurements, and the collection of samples from different layers of the weathering profile. Samples are selected based on noticeable vertical and horizontal changes. These samples are described in the field and through megascopic analysis to create a representation of the weathering profile's different layers. Additionally, the samples are used to prepare polished slabs and thin sections for microscopic examination. The data gathered from both fieldwork and laboratory analysis is used to prepare the manuscript.

3. Regional geology

The study area is situated in Al Quayiah along the Jeddah-Riyadh highway, where the Arabian Shield rocks meet the overlying Phanerozoic sedimentary succession. In central Saudi Arabia (Figs. 1A, 1B, 2A, 2B, and 2C), the Precambrian Arabian Shield rocks are covered by the Phanerozoic sedimentary succession, specifically the Khuff Formation from the Permo-Triassic period. The Precambrian rocks consist of metamorphosed and highly folded metamorphic and igneous rocks. In contrast, the younger Phanerozoic carbonate rocks of the Khuff Formation are only slightly folded and not metamorphosed. According to Johnson's (2006) Arabian Shield map, the eastern part of the Arabian Shield rocks comprises several rock units, listed from oldest to youngest (Fig. 2B).

3.1. Unassigned Neoproterozoic rocks

These map units consist of intrusive rocks that are not assigned to any specific lithostratigraphic units due to the lack of direct dating and unclear information about their relative positions within the rock layers. These include unassigned dioritoids, gabbros, and serpentinites.

3.2. Cryogenian layered rocks

3.2.1. Al Amar Group, aged over 690 million years (Ma)

The Al Amar group crops out in the Ar Rayn terrane in the eastern part of the shield, bounded by the Al Amar fault on the west and the Phanerozoic unconformity on the east. Stacey et al. (1984) and Stoeser and Stacey (1988) suggested that the group is >670 Ma. The group is notable for hosting small VMS occurrences, epithermal gold deposits (for example, Al Amar mine), and a significant Zn occurrence (Khnaighyiah) (Doebrich et al., 2007). The rocks are commonly greenschist facies, but in the east are amphibolite-facies schist and paragneiss. Typical rock types include andesitic tuff and breccia, andesite flow rock, well-bedded andesitic and rhyolitic tuff, welded rhyolitic tuff, minor calcareous dolomite and siltstone, and pyritic chert. The higher-grade rocks are phyllite, quartz-feldspar schist, biotite-amphibole schist, calc schist, amphibolite, amphibole and garnet-bearing paragneiss, and leucocratic quartz-feldspar gneiss.

3.3. Crygenian intrusive rocks

3.3.1. Najirah granite, 640-575

Johnson (2005) named this map unit (nr) after the Najirah batholith in the Ad Dawadimi source map. The granite intrudes the Abt formation along the axis of the Ad Dawadimi terrane as a heterogeneous body ranging in composition from tonalite to granodiorite to monzogranite.

3.4. Cryogenian-Ediacaran layered rocks

3.4.1. Abt Formation, age uncertain

This map unit (bt) underlies a large part of the Ad Dawadimi terrane in the eastern part of the shield. The formation consists of thin- to medium-bedded fine-grained sandstone and siltstone, which are metamorphosed to the lower greenschist facies and are present as quartz-biotite-chlorite-rich rocks with granoblastic and phyllitic textures. It is tentatively interpreted as a late terrane-forming rock unit and may represent deposition in a forearc basin during the final convergence of East Gondwana (Collins and Pisarevsky, 2005).

3.5. Crygenian-Ediacaran intrusive rocks

3.5.1. Syn- to post-Al Amar intrusives, 690-615 Ma

This map unit (alx), named by Johnson (2005), consists of igneous rocks exposed in the Ar Rayn terrane at the eastern margin of the shield. They intruded the Al Amar group during its deposition or soon after and are directly dated between 689 Ma and 616 Ma (Doebrich et al., 2007). This age range is large, but the available geochronology does not allow finer divisions. The rocks include tonalite, quartz diorite, diorite, gabbro, and minor trondhjemite. Where strongly deformed, particularly close to the Phanerozoic unconformity at the edge of the shield, the intrusives are represented by interlayered amphibole orthogneiss and chlorite-epidote schist.
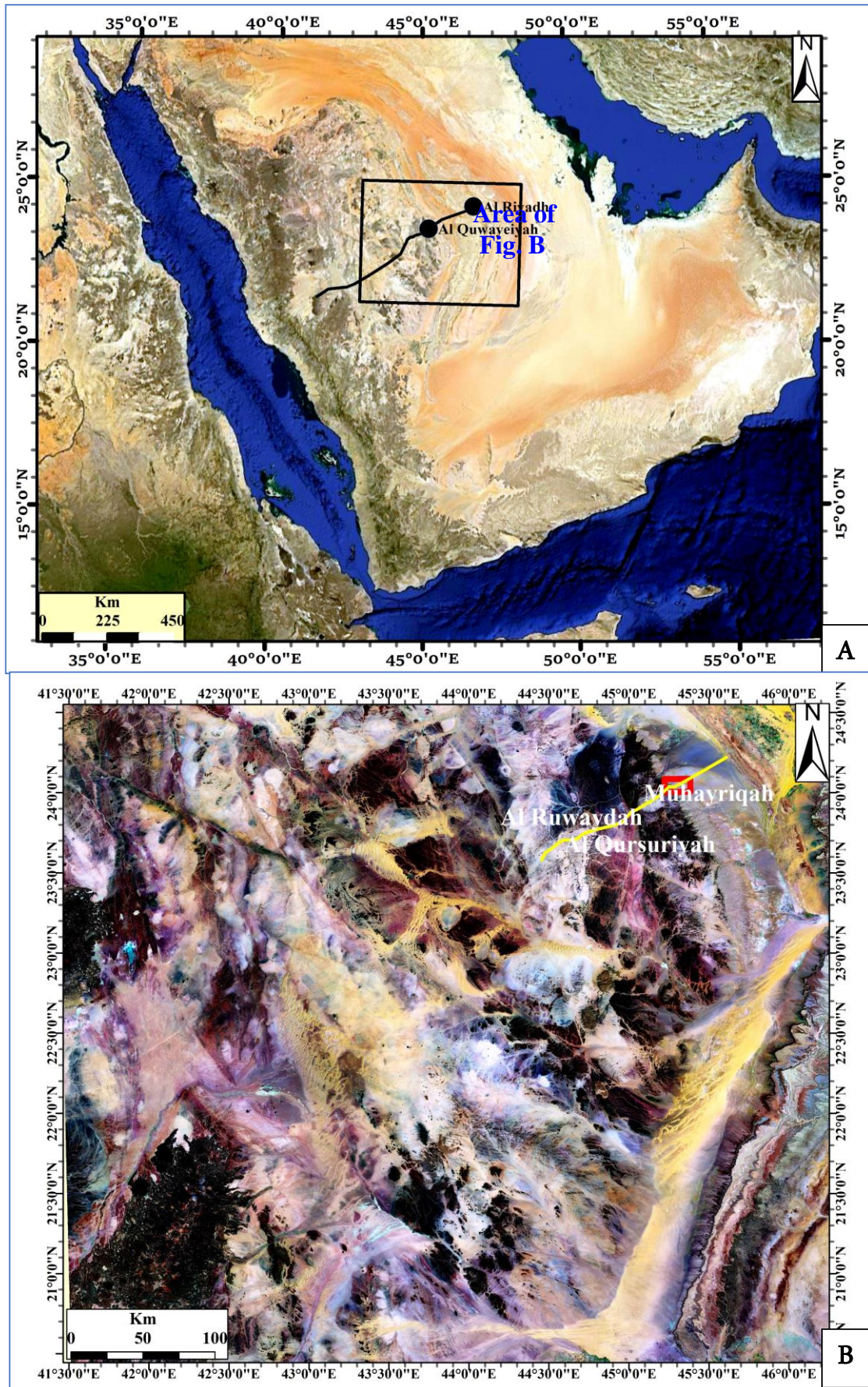
Fig. 1: A: Regional satellite image of Saudi Arabia; B: Detailed Satellite image of Al Quwayyiah-Al Riyadh area
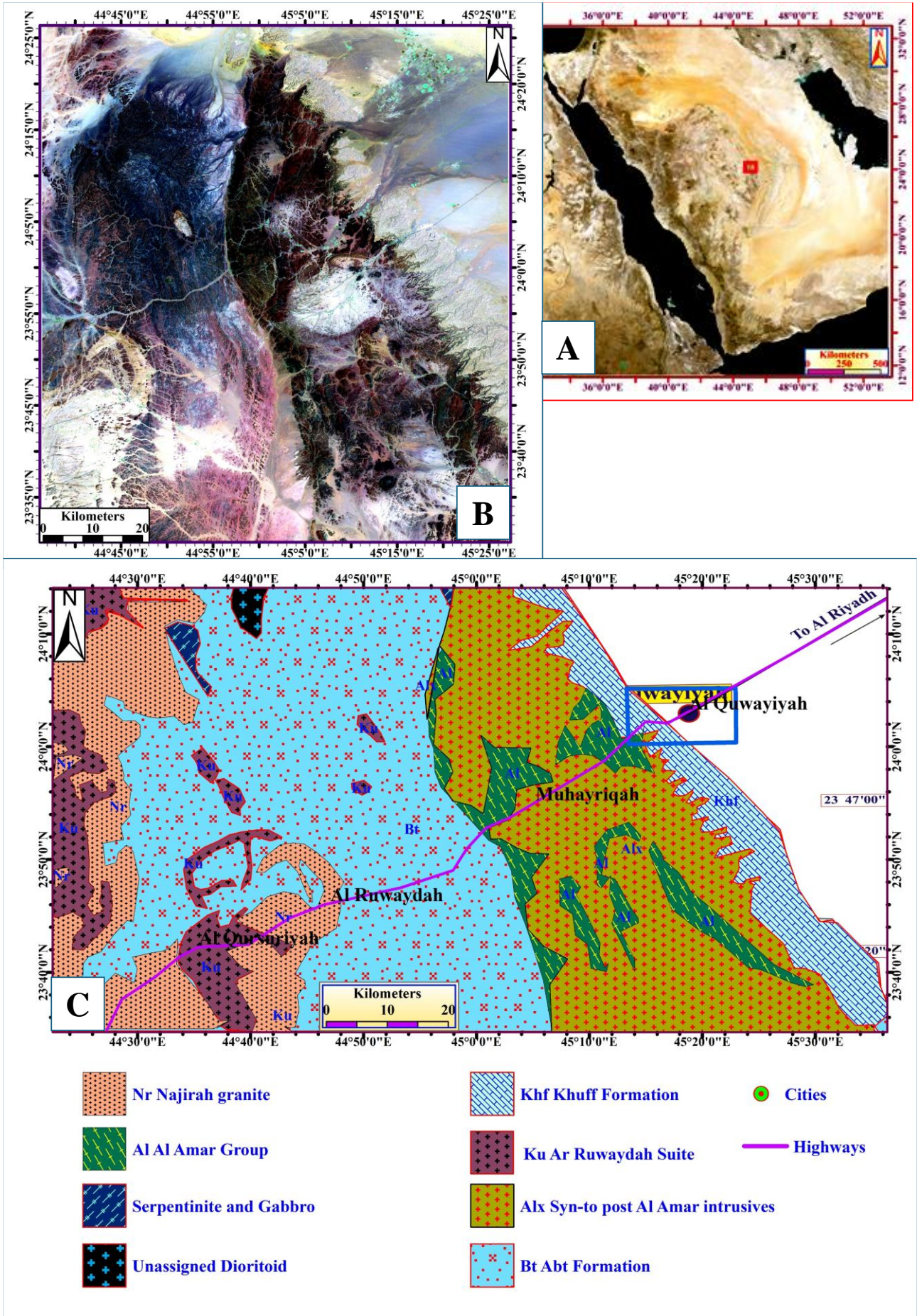
Fig. 2: A: Satellite image of Saudi Arabia; B: Satellite image of Al Quwayyiah area; C: Geologic map of Al Quwayyiah area (Johnson, 2006)

3.6. Ediacaran intrusive rocks

3.6.1. Ar Ruwaydah suite, 605-565 Ma

The suite includes Khurs Granite and Arwa Granite. They are distinct from the Abanat suite due to their pale gray to white color and the absence of tin-tungsten or niobium-lanthanum-rare-earth-element minerals. According to Johnson (2005), Khurs Granite is mainly leucocratic monzogranite, with some syenogranite and biotite-muscovite aluminous granite. This granite is undeformed and forms prominent inselbergs (isolated hills).

3.7. Paleozoic-Mesozoic

3.7.1. Phanerozoic rocks (Khuff Formation)

The studied Fe-laterite horizon is directly overlain by a succession of thinly bedded ferruginous mudstones, siltstones, and sandstones. This succession ranges from 25 to 40 meters thick and becomes more thickly bedded from the lower to the middle and upper parts. At the top of this red siliciclastic zone, there is a yellow bedded dolostone unit. These two units are part of the Khuff Formation, which dates to the Jurassic period.

3.8. Local geology of Al Quwayyiah

In this area, the Arabian Shield rocks consist of syn- to post-Al Amar intrusives. Chemical weathering of these rocks has led to the formation of a Fe-rich laterite profile. The geologic map of this area is shown in Fig. 3. The white carbonate rocks of the Khuff Formation can be seen directly overlying the red weathered mafic rocks of the Arabian Shield (Figs. 2, 3, 4, and 5).

4. Description of Fe-laterite profile

The weathering profile is generally friable and clay-like, with irregular contact with the overlying carbonates of the Khuff Formation (Fig. 4A and 4B). The studied Fe-laterite profile (Fig. 5) has three main zones. The current Fe-laterite zone, which is 3-10 meters thick, is found at the contact between the Permo-Triassic carbonates of the Khuff Formation and the Precambrian mafic quartz diorite and gabbros of the Arabian Shield, specifically from the syn- to post-Al Amar intrusives. The weathering profile developed from the parent crystalline mafic rocks shows a clear, gradual transition. Field observations and measurements revealed different weathering zones within this Fe-laterite horizon. From bottom to top, these zones are the parent mafic intrusive rocks (quartz diorite and gabbros) and the overlying slightly to highly altered horizons (Fig. 5). These horizons were systematically described and sampled, with the collected samples undergoing detailed mega- and microscopic analysis.

5. Megascopic description of the weathering profile

The parent rocks, quartz diorite and gabbro, are holocrystalline, hard, and dark green. These greenish-black parent rocks are almost massive, while the overlying Fe-laterite horizons are red and friable. The slightly altered rocks are reddish-green, hard, and composed of semicrystalline greenish-white and red interlocked crystals (Figs. 6B, 7A, and 7B). The green minerals show some alignment (Figs. 7A and 7B). In the highly altered horizon, the green iron silicate minerals gradually disappear, and the rocks are made up of mottled brownish-black and blood-red minerals (Fig. 7C). Toward the upper parts of this horizon, the rocks become homogeneous and consist of massive red Fe-silicate minerals (Fig. 7D).

6. Microscopic description of the weathering profile

Under the microscope, the parent rocks are mainly composed of hornblende, chlorite, feldspars, quartz, and epidote (Fig. 8). Chlorite appears as either fine-grained light green aggregates filling the spaces between coarser hornblende and feldspar aggregates or as euhedral to subhedral dark coarse grains. Quartz is present as individual light grey grains or as clusters associated with feldspars. Microscopic examination of the different weathering horizons showed a progressive upward alteration and destruction of the parent Fe-silicate minerals.

The parent rocks are composed of holocrystalline quartz diorite and gabbro (Figs. 8A and 8B), with interlocked hornblende, quartz, and plagioclase feldspars (Appendix A, Fig. A1A and Figs. 8A and 8B). Some black iron oxide patches are observed replacing green hornblende crystals. In this horizon, most green hornblende crystals are pseudomorphically replaced by chlorite, hematite, and goethite (Figs. 8C and 8D). The feldspars consist of orthoclase with microcrystalline aggregates (Fig. 8D) and show slight kaolinization and sericitization (Fig. 8B). The Fe-silicate minerals vary in crystal size, with small green aggregates intermixed with microcrystalline quartz (Figs. 9A and 9B). Large quartz crystals are slightly fractured and replaced by hematite and goethite minerals (Figs. 9A and 9B).

In the initial stages of alteration (stage I; Appendix A, Fig. A1B), many hornblende crystals become progressively chloritized, leaving small, cleavable, slightly hematitized crystals (Appendix A, Figs. A1A and A1B). The resulting chlorite patches are isotropic (Figs. 9C and 9D), and quartz domains become slightly chloritized (Figs. 9C and 9D).
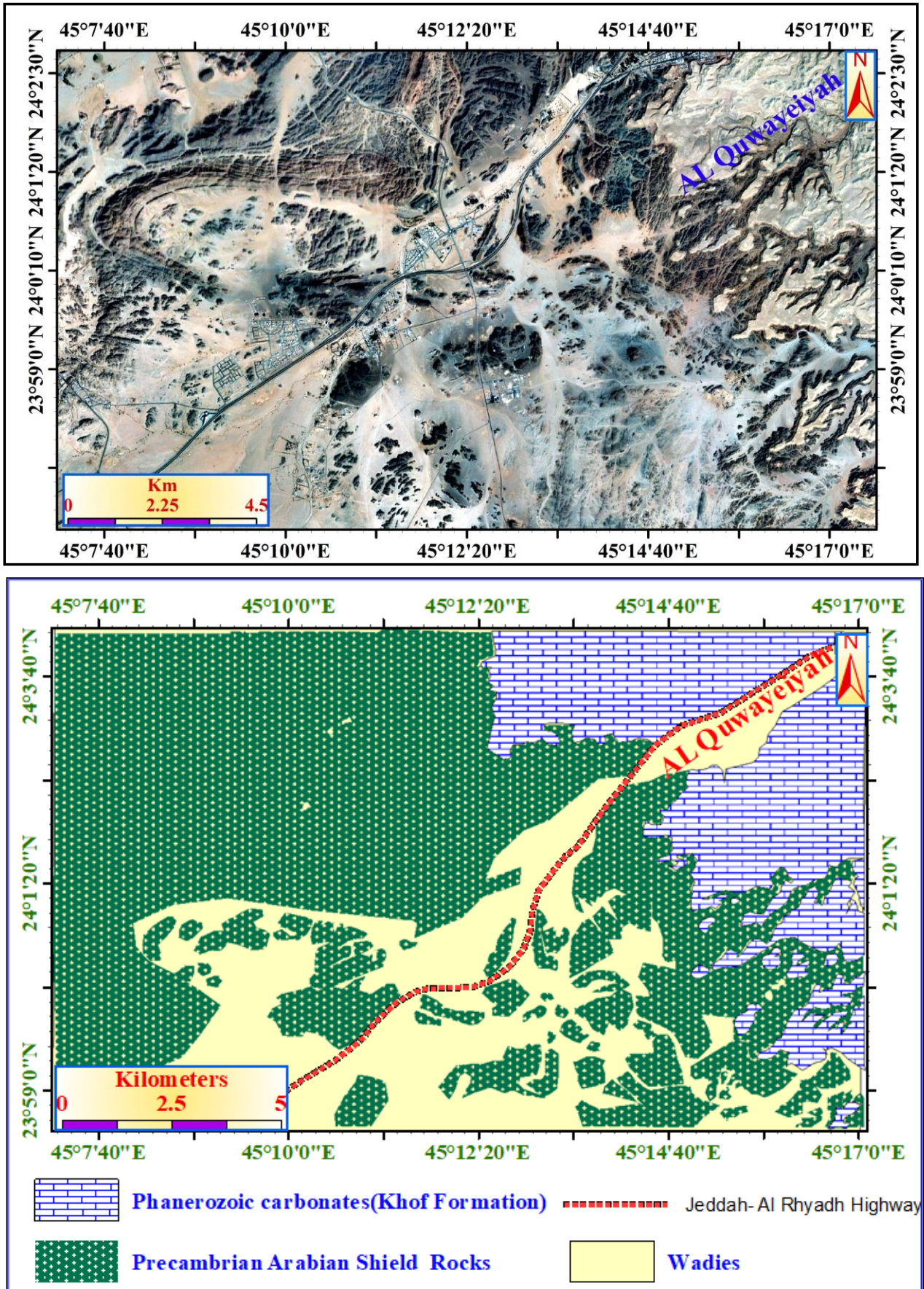
Fig. 3: Detailed satellite image of the Arabian Shield and the overlying carbonates (Upper); Simplified geologic map of the satellite image showing the presence of the carbonates of Khuff Formation directly on the Arabian Shield rocks (Lower)
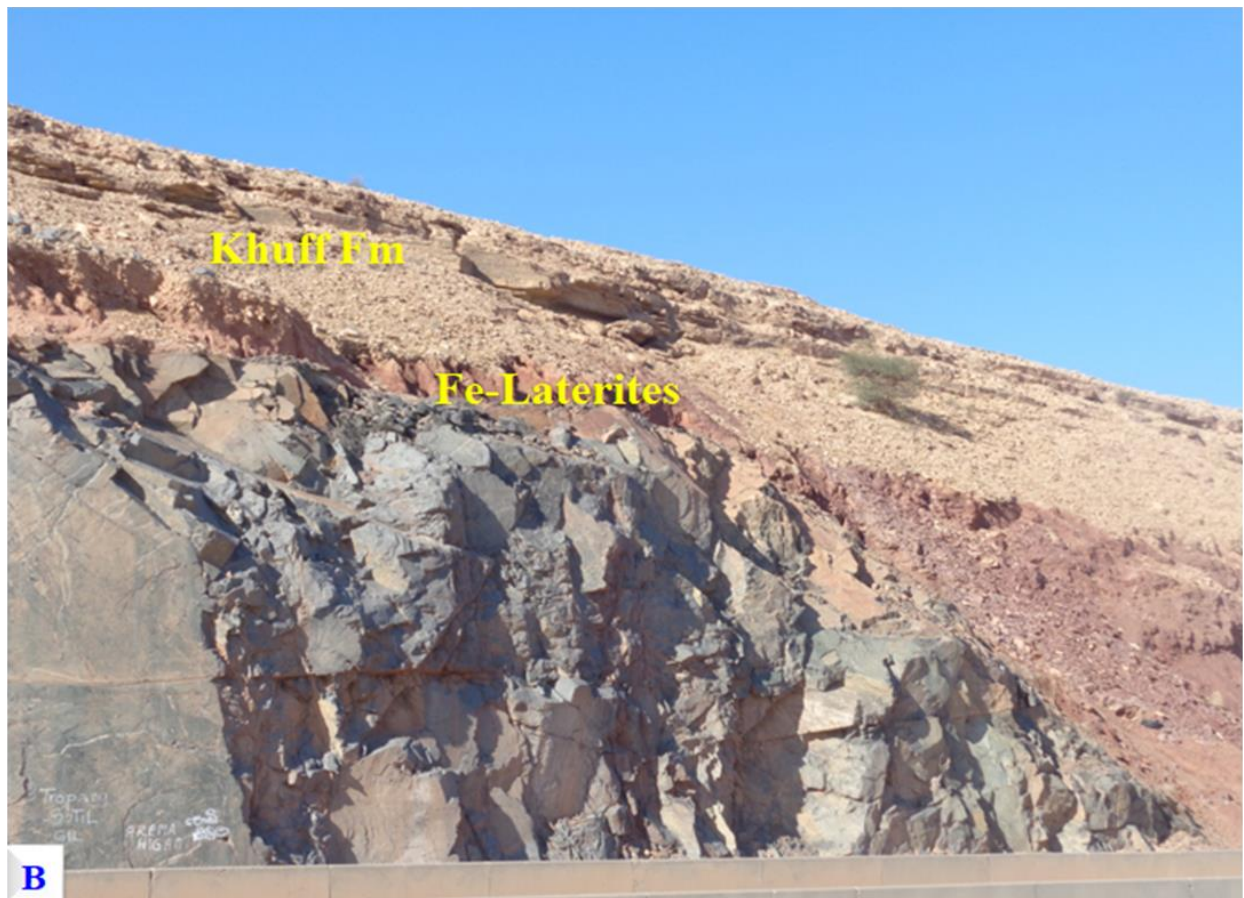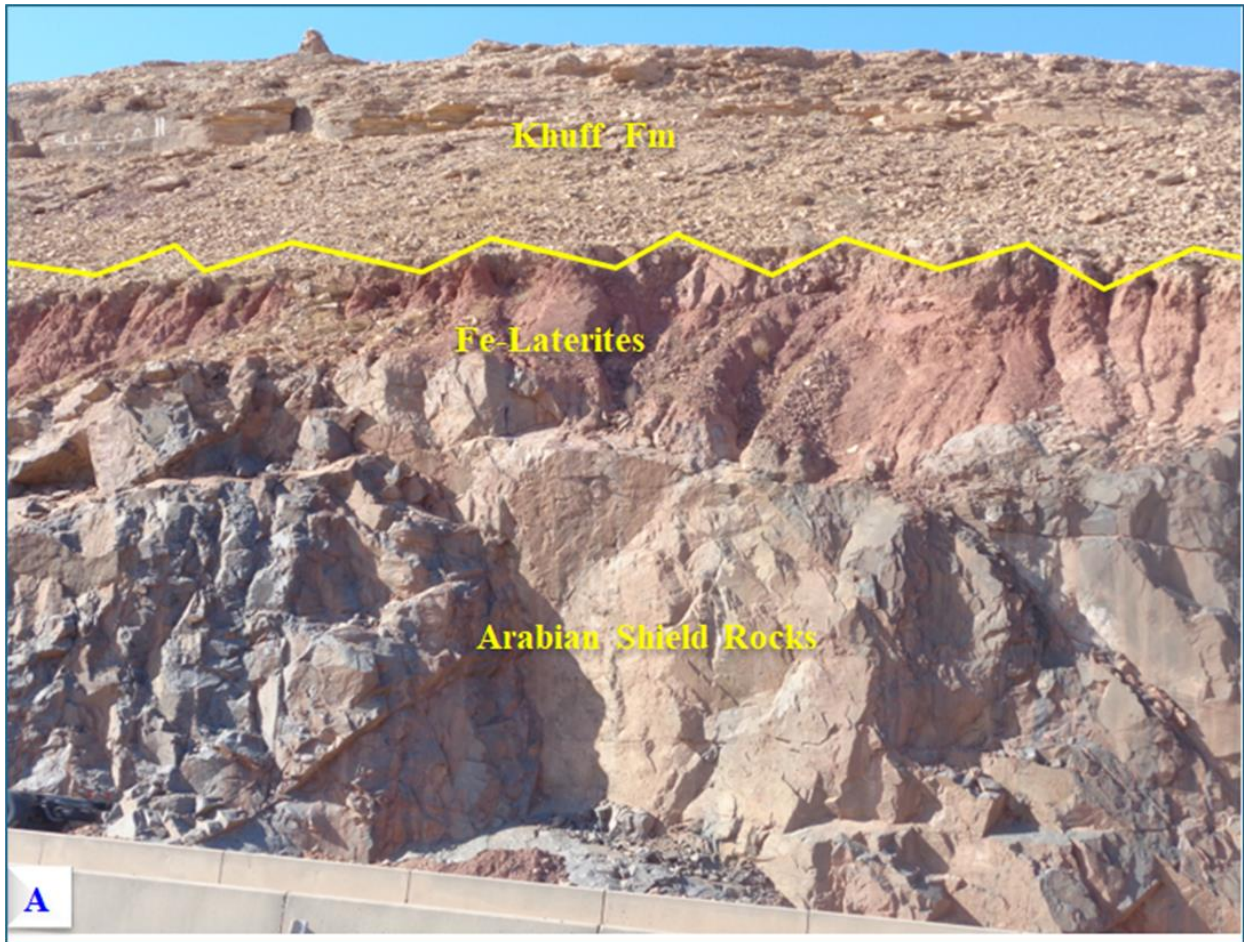
Fig. 4: Field photos of the white carbonates of A: Khuff Formation on the B: black Arabian Shield rocks
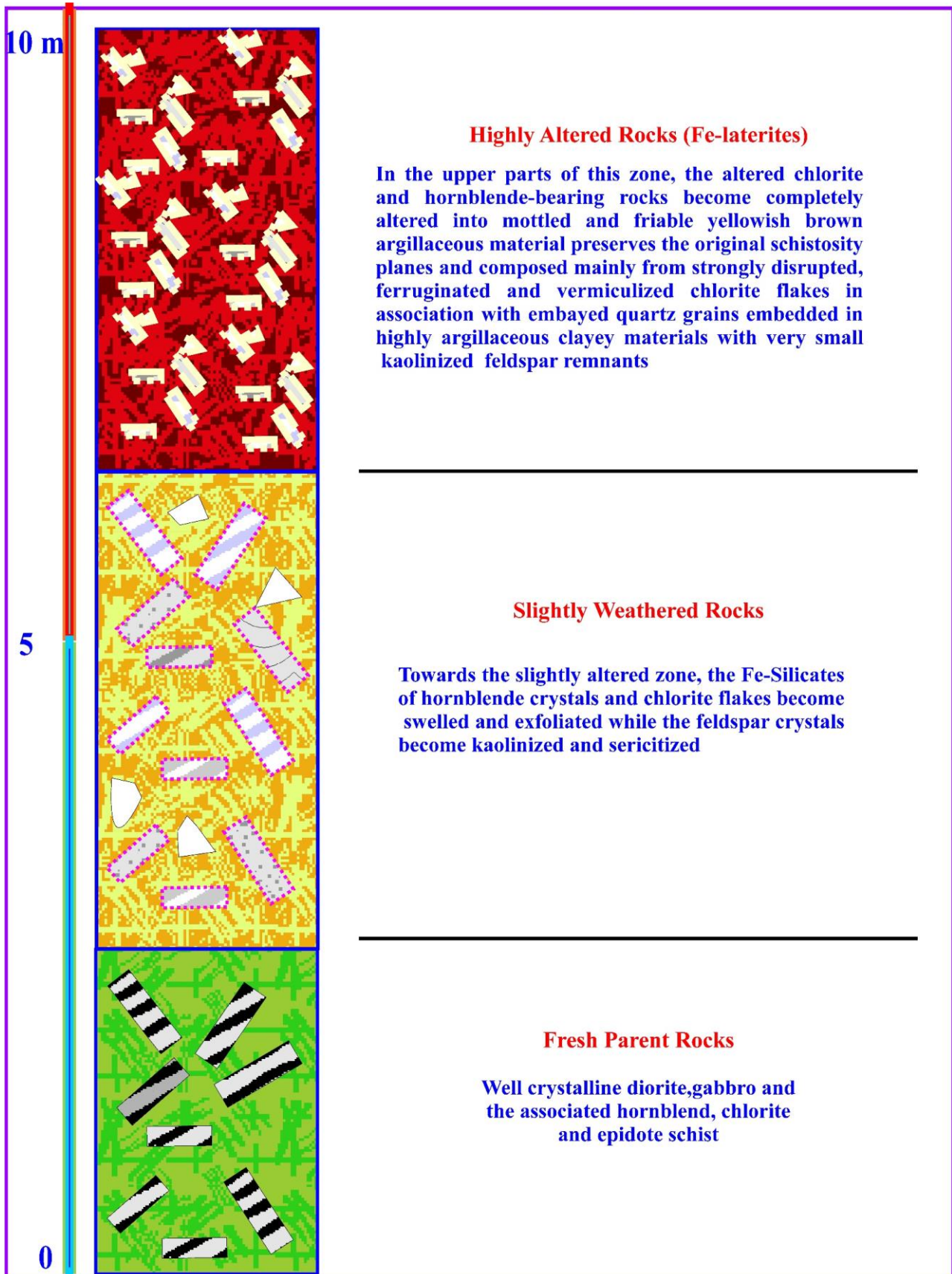
10 m

5

0

Highly Altered Rocks (Fe-laterites)

In the upper parts of this zone, the altered chlorite and hornblende-bearing rocks become completely altered into mottled and friable yellowish brown argillaceous material preserves the original schistosity planes and composed mainly from strongly disrupted, ferruginated and vermiculized chlorite flakes in association with embayed quartz grains embedded in highly argillaceous clayey materials with very small kaolinized feldspar remnants

Slightly Weathered Rocks

Towards the slightly altered zone, the Fe-Silicates of hornblende crystals and chlorite flakes become swelled and exfoliated while the feldspar crystals become kaolinized and sericitized

Fresh Parent Rocks

Well crystalline diorite, gabbro and the associated hornblend, chlorite and epidote schist

Fig. 5: The different horizons of the weathering profile

Fig. 6: A: Field photo showing the irregular contact between the Fe-laterite profile (red, lower) and the overlying carbonates of Khuff Formation (white, upper); B: Hand sample of the hard, slightly weathered mafic crystalline rock

During the progressive stages of alteration (stage II, Appendix A, Fig. A1C), hornblende crystals exfoliate and swell with the growth of inter-cleavage black iron oxide laminae parallel to the cleavage planes (Figs. 10A and 10B). Some hornblende crystals undergo quick and complete hematitization (Figs. 10A and 10B). The massive chlorite domains formed in stage I show progressive hematitization, forming blood red iron oxyhydroxides and hematite shreds (Appendix A, Figs. A1A and A1B). Further

alteration (stage III, Appendix A, Fig. A1D) leads to the formation of a complete blood red Fe-oxyhydroxide phase on the altered hornblende crystals from stage II. In this stage, the crystal outlines and hematitized cleavage planes are still preserved but are now red (Figs. 10C and 10D). Kaolinized feldspars and associated microcrystalline aggregates become stained with iron oxyhydroxides (Figs. 10C and 10D). In stage IV (Appendix A, Fig. A1E) of alteration, ferruginated hornblende crystals become dehydrated and recrystallized, with iron oxyhydroxides progressively turning into reddish-brown to black goethite and hematite, forming large domains that include more than one crystal (Fig. 11A and 11B). Some black hematite patches and domains form in place of the amorphous iron oxyhydroxides phase (Figs. 11A and 11B). In the final stages of hematitization (stage V), blood red (goethite) and black (hematite) minerals form instead of the previously hematitized and chloritized hornblende crystals (Figs. 11C and 11D). Small green and blood-red relics are still preserved (Figs. 11C and 11D).

Ultimate stages of hematitization (stage VI, Appendix A, Fig. A1F) led to the complete disappearance of the cleavage planes of the euhedral hematitized hornblende crystals and the formation of earthy amorphous iron oxyhydroxide phase along these planes (Figs. 12A and 12B). This stage of alteration is associated with the formation of semicircular light color Al-rich domains (Figs. 12A and 12B). These domains are stained with the blood-red iron oxyhydroxides (Figs. 12C and 12D). This is accompanied by the formation of microcrystalline quartz aggregates (Figs. 12C and 12D).

7. Discussion and conclusions

The parent diorite and gabbro are composed of plagioclase, hornblende, and quartz. The hornblende is heavily chloritized, and the quartz grains are very angular. The slightly altered horizon, which is 1-1.5 meters thick, is mottled, friable to hard, and brownish-green. It preserves most of the original mineralogical and petrographic characteristics of the parent rock. This horizon is similar to the "lithomarge" or "structure conserve" described in French literature and the "saprolite" horizon in English literature. The initial stages of alteration are marked by the appearance of cloudy, earthy material mixed with Fe-oxyhydroxides and the transformation of green chlorite flakes and hornblende crystals into yellowish-green. These stages of alteration correspond to the "degradation" process described by Millot (1964), where the original double-chain phyllosilicate structure of hornblende and chlorite is preserved.

Fig. 7: A, B: Hand samples of the reddish-green slightly weathered crystalline mafic rocks (quartz diorite and gabbro); C: Mottled highly altered rocks of interlocked red-brown and blood red domains; D: Highly altered homogenous rock of massive to argillaceous nature and rich in iron
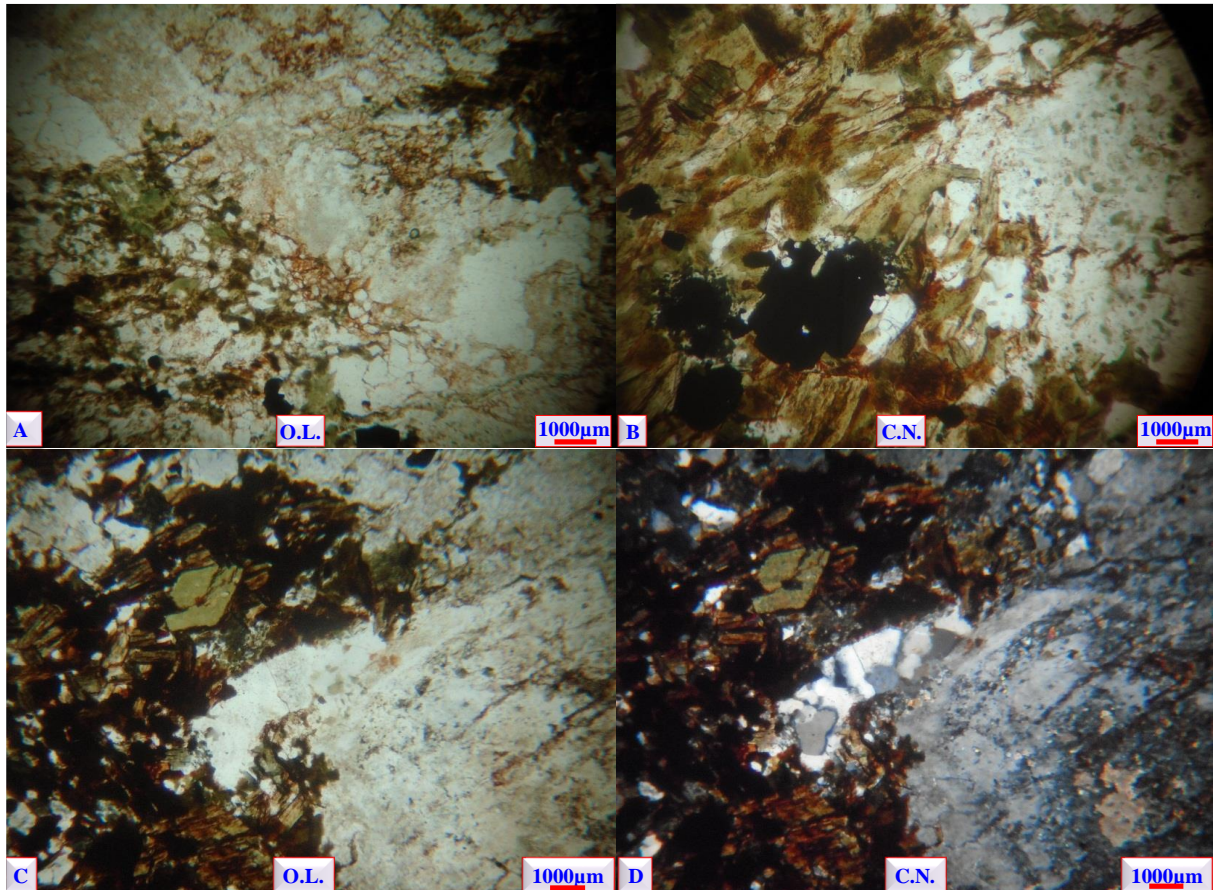
Fig. 8: A, B: The parent mafic rocks of the Arabian Shield composed of hornblende, feldspars, and quartz. O.L. = Ordinary Light; C.N. = Crossed Nicols. C, D: The parent mafic rocks of the Arabian Shield composed of hornblende, feldspars, and quartz
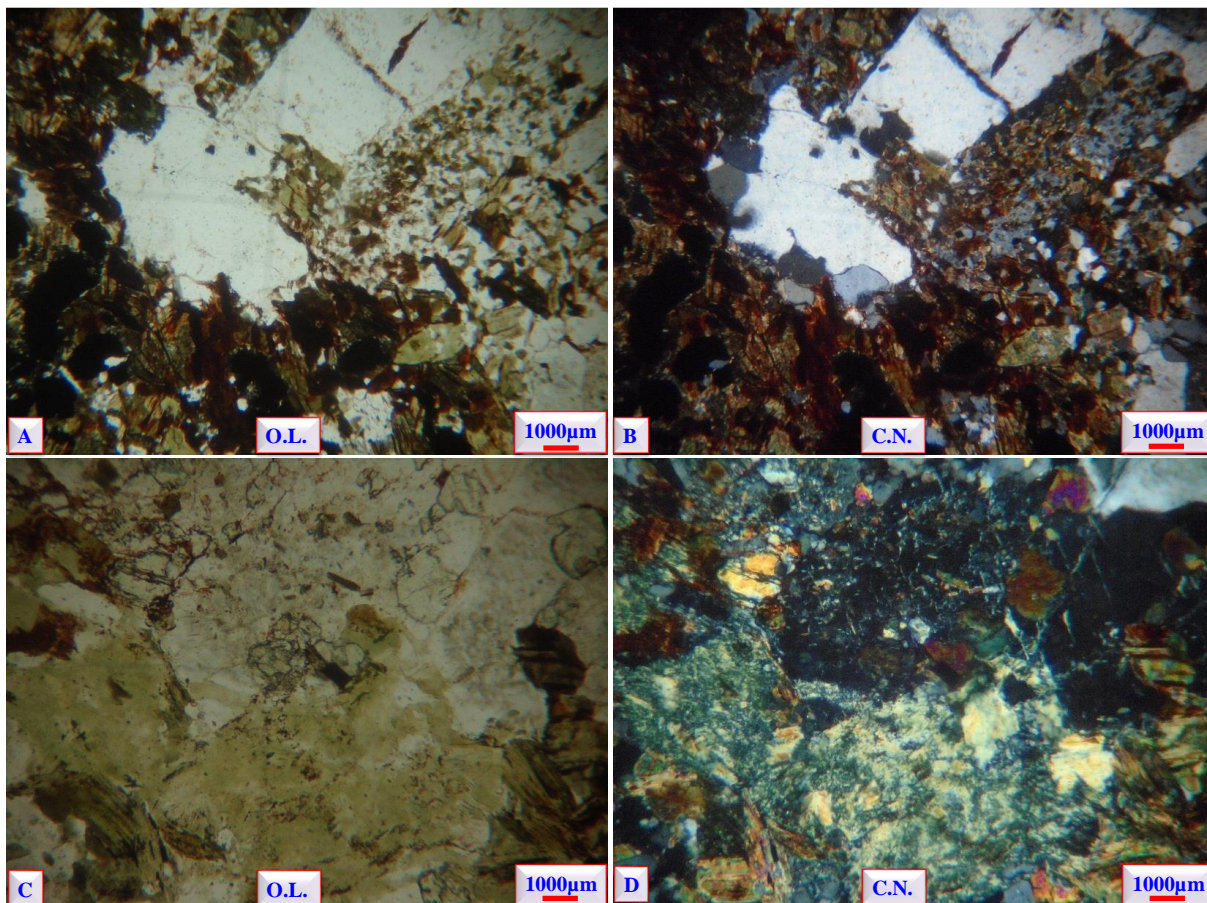

Fig. 9: A: The Fe-silicate minerals show clear variation in crystal size, with small green aggregates intermixed with microcrystalline quartz. B: Large quartz crystals are slightly fractured and replaced by hematite and goethite minerals. C, D: Chlorite domains formed by the chloritization of hornblende in the initial stages of alteration (central part of the photo)
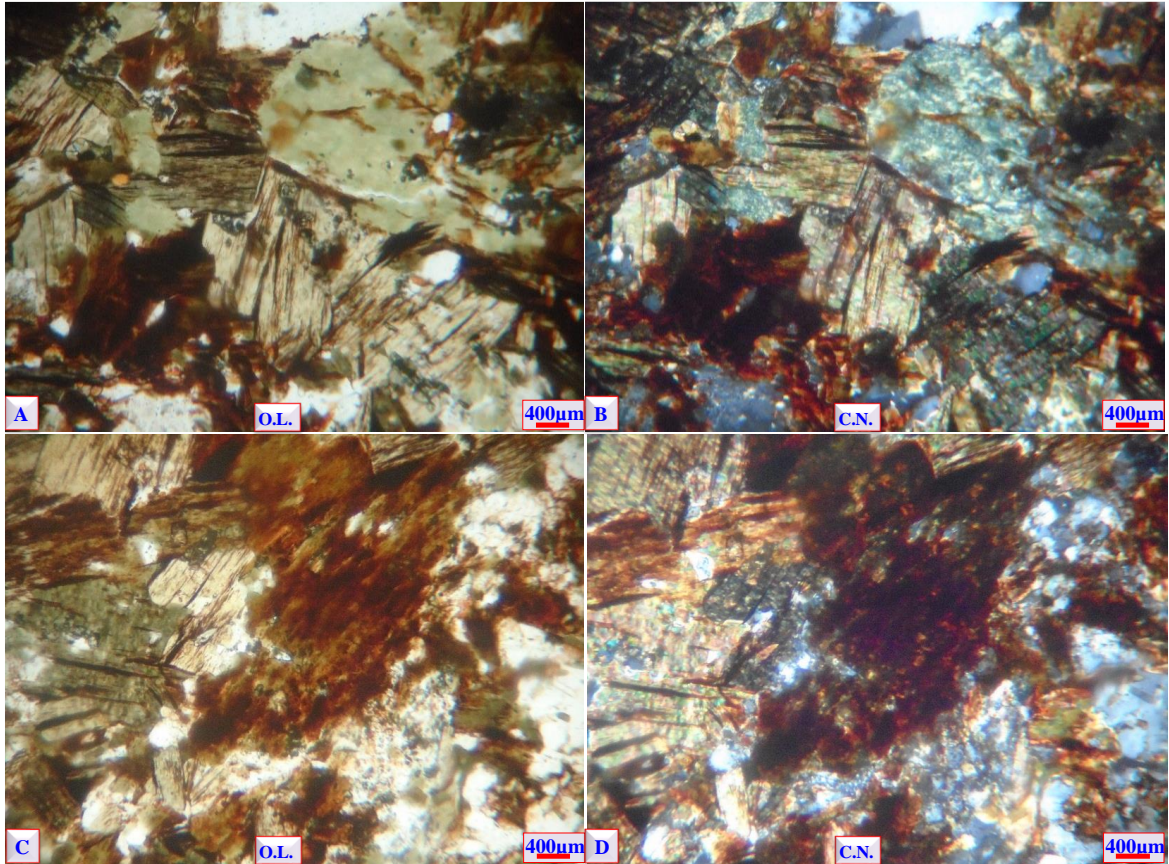
Fig. 10: A, B: The hornblende crystals become exfoliated and swell, with inter-cleavage black iron oxide laminae growing parallel to the cleavage planes. Some hornblende crystals show rapid and complete hematitization. C, D: Blood red and chlorite, respectively
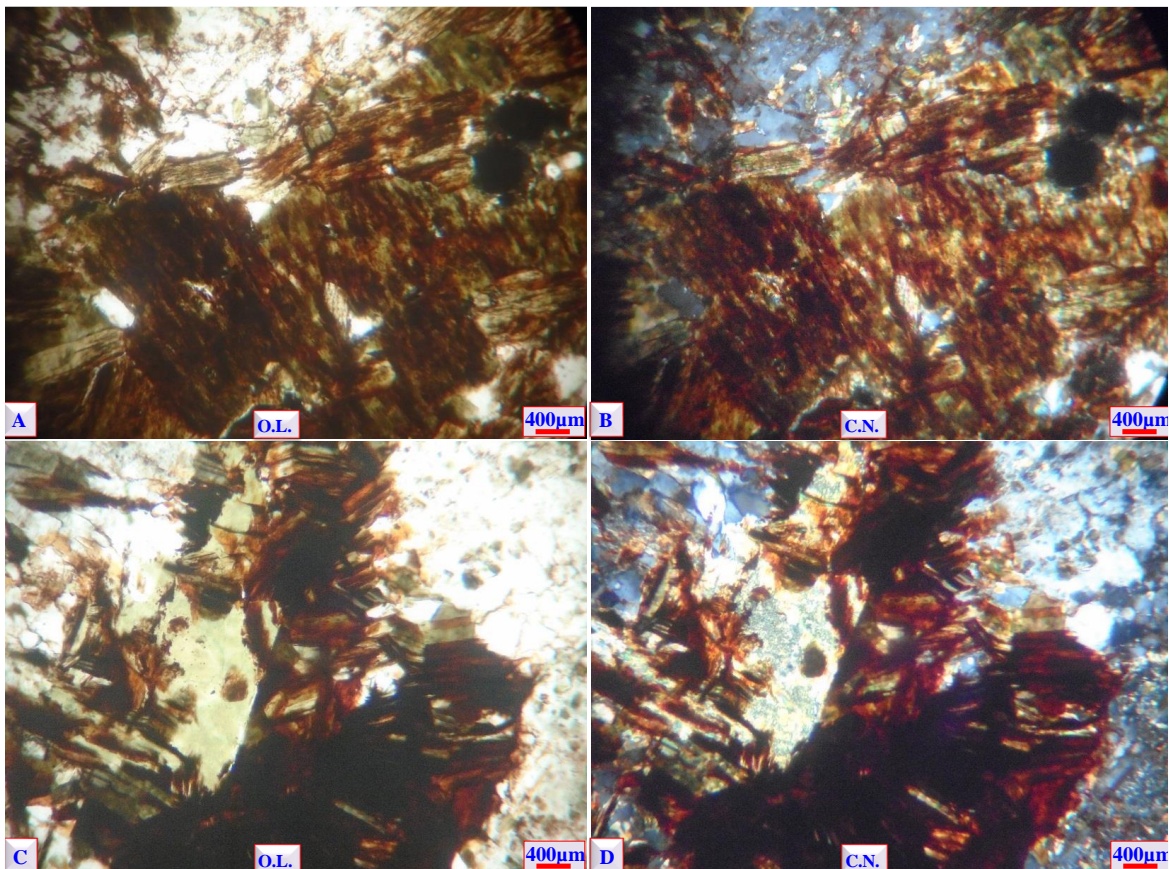

Fig. 11: A, B: Ferruginated hornblende crystals become dehydrated and recrystallized, with the formed iron oxyhydroxides progressively turning into reddish-brown to black goethite and hematite, creating large domains that include more than one crystal. C, D: In the ultimate stages of hematitization (stage V), blood red (goethite) and black (hematite) form in place of the previously hematitized hornblende crystals. Small green and blood-red relics are still preserved

In this stage of alteration, quartz, epidote, and feldspars are slightly altered. Towards the top of this horizon, the remaining Fe-silicate minerals show strong curling and fragmentation. The surrounding argillic plasma mainly consists of intermixed dark Fe-oxyhydroxides (ferrihydrites) and light Al- and Si-rich gel with fewer small quartz grains. The feldspar crystals become completely kaolinized and sericitized. In the final stages of alteration, the interstitial Fe accumulations form thin parallel hematite bands and lamellae along the cleavage planes of the original Fe-silicates. The remaining ferruginated and swollen chlorite and hornblende crystals become completely masked by the enclosing Fe-oxyhydroxides and hematite, ultimately being entirely pseudomorphosed by hematite. Quartz grains are partially to completely corroded by the enclosing Fe-oxyhydroxides and hematite matrix, though in some areas, the quartz grains remain in contact.

The progressive stages of hematitization and the formation of new minerals during weathering include:

a) Pseudomorphoses by transformation or degradation: During the initial stages of hydrolysis and oxidation of the Fe-silicate minerals, hornblende crystals swell and exfoliate. The cleavage planes become filled with blood-red iron-oxyhydroxides and hematite.

b) Pseudomorphoses by neoformation: In the final stages of Fe-silicate mineral alteration, the internal structure of these minerals is completely destroyed. New mineral phases such as goethite, hematite, and kaolinite form instead of the amorphous iron-oxyhydroxides from stage a. The entire rock becomes more friable and clay-like.

c) Pseudomorphoses by secondary accumulation: During this stage, secondary lateritization occurs, forming kaolinite populations due to the downward migration of silicon and an increased Al/Si ratio in the light amorphous Al- and Si-rich gel material in the upper parts of the weathering profile. Mosaic and microcrystalline quartz aggregates form from the precipitation of leached silicon from the upper parts of the Fe-laterite horizon.
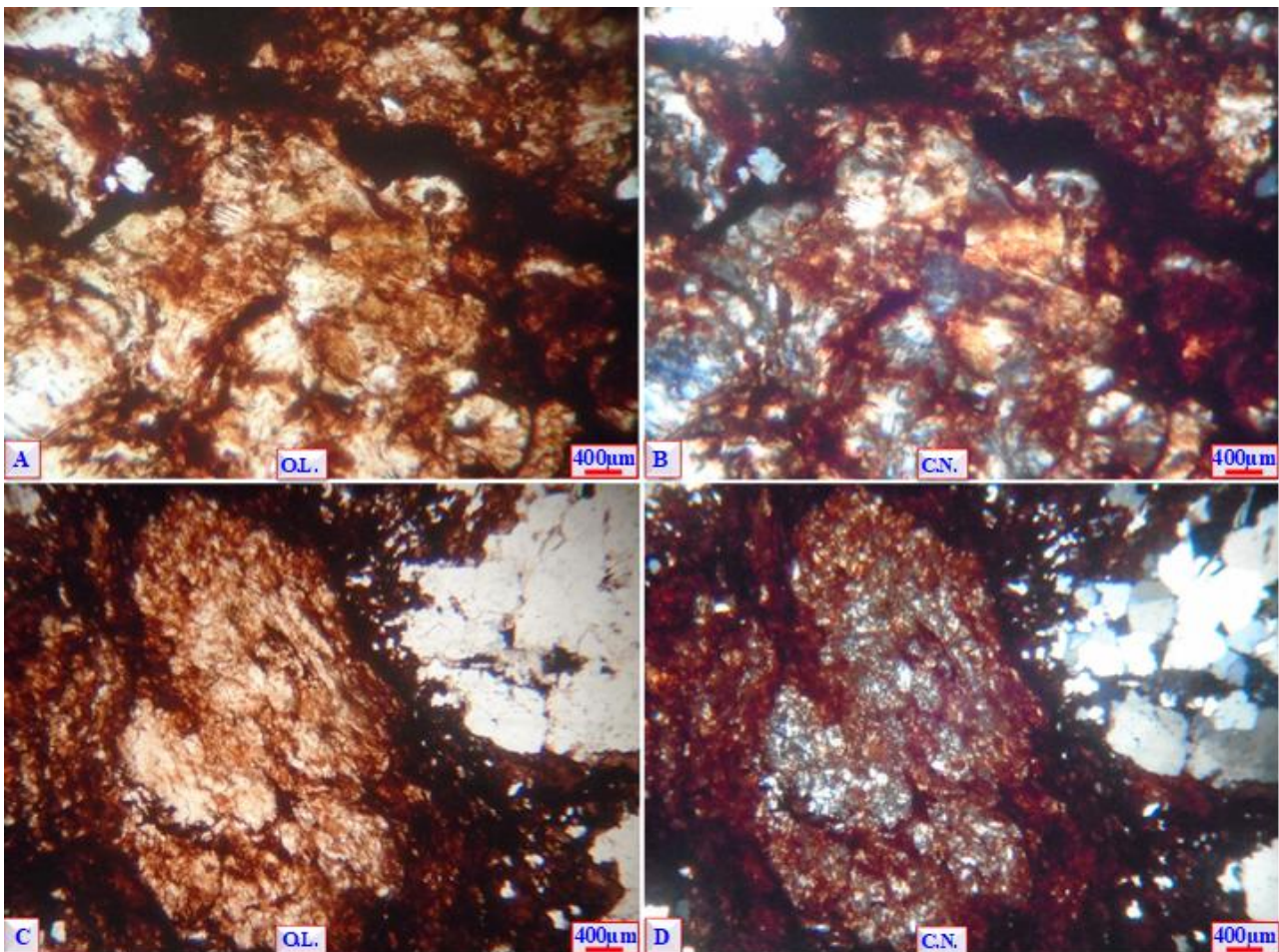

Fig. 12: A, B: In the ultimate stages of hematitization (stage VI), the cleavage and euhedral shapes of the hematitized hornblende crystals completely disappear, resulting in the formation of an earthy, amorphous iron oxyhydroxide phase. This stage of alteration is associated with the formation of white, semicircular Al-rich domains. C, D: White, semicircular Al-rich domains are stained with blood-red iron oxyhydroxides and intermixed with some microcrystalline quartz aggregates

Appendix A. Petrographic and mineralogic evolution

Petrographic and mineralogic evolution of the different horizons of the studied Fe-laterite profile.
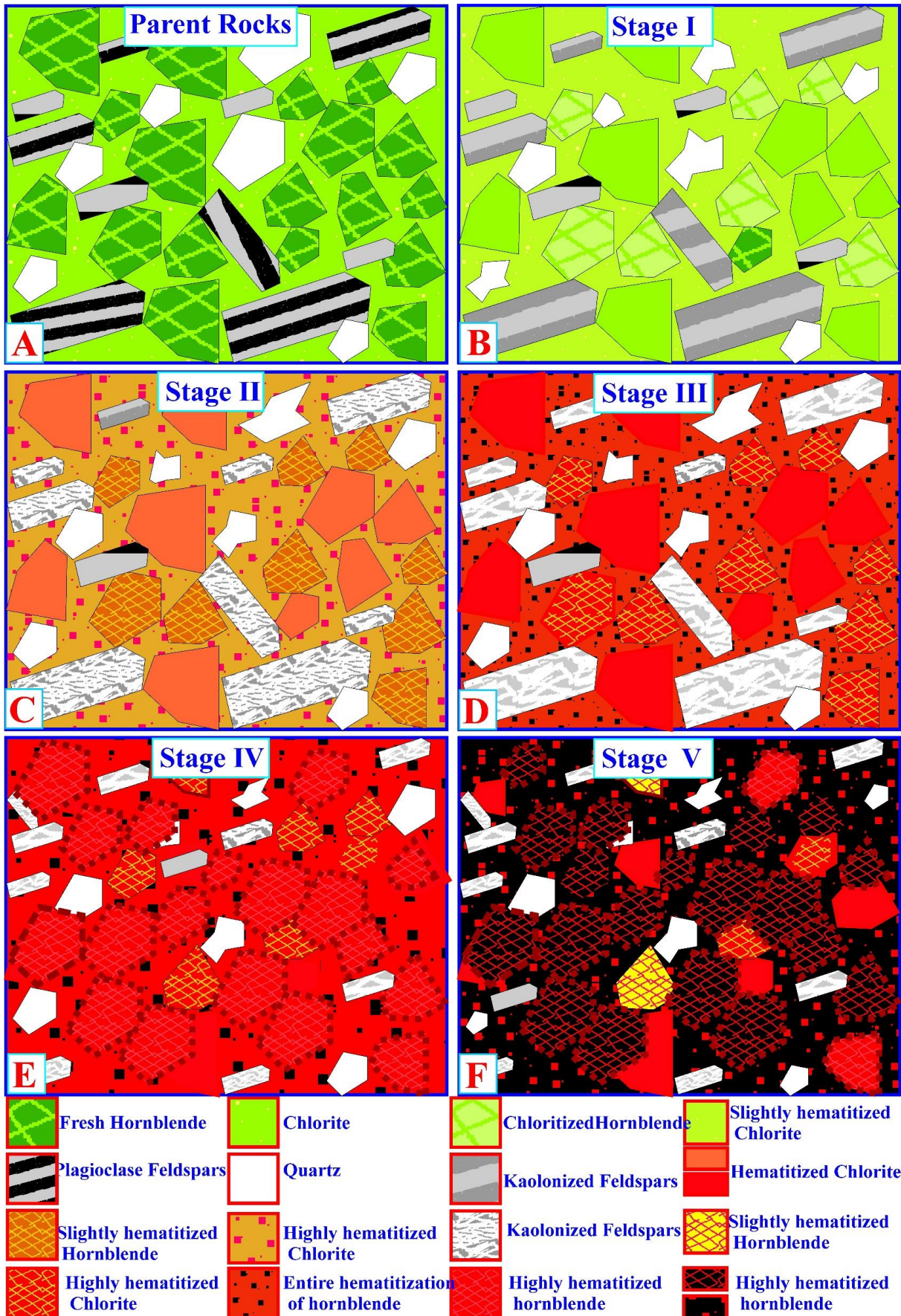

Fig. A1: A: Parent unaltered rocks; B: Slightly altered horizon (stage I); C, D: Moderately altered horizon (stages II, III); E, F: Highly altered horizon (Fe-laterites, stages IV, V)

Compliance with ethical standards

Conflict of interest

The author(s) declared no potential conflicts of interest with respect to the research, authorship, and/or publication of this article.

References

Berner RA and Schott J (1982). Mechanism of pyroxene and amphibole weathering; II, Observations of soil grains. American Journal of Science, 282(8): 1214-1231. https://doi.org/10.2475/ajs.282.8.1214

Berner RA, Sjöberg EL, Velbel MA, and Krom MD (1980). Dissolution of pyroxenes and amphiboles during weathering. Science, 207(4436): 1205-1206. https://doi.org/10.1126/science.207.4436.1205 **PMid:17776857**

Collins AS and Pisarevsky SA (2005). Amalgamating eastern Gondwana: The evolution of the Circum-Indian Orogens. Earth-Science Reviews, 71(3-4): 229-270. https://doi.org/10.1016/j.earscirev.2005.02.004

Doebrich JL, Al-Jehani AM, Siddiqui AA, Hayes TS, Saleh Y, Wooden JL, and Al-Shammari A (2007). Geology and mineral resources of the Ar Rayn terrane, eastern Arabian Shield, Kingdom of Saudi Arabia. Precambrian Research, 158: 17-50. https://doi.org/10.1016/j.precamres.2007.04.003

Dong H, Peacor DR, and Murphy SF (1998). TEM study of progressive alteration of igneous biotite to kaolinite throughout a weathered soil profile. Geochimica et Cosmochimica Acta, 62(11): 1881-1887. https://doi.org/10.1016/S0016-7037(98)00096-9

Drever JI (1971). Chemical weathering in a subtropical igneous terrain, Rio Ameca, Mexico. Journal of Sedimentary Research, 41(4): 951-961. https://doi.org/10.1306/74D723C4-2B21-11D7-8648000102C1865D

El Aref MM (1993). Pedogenesis and related gibbsite and natroalunite formation in Um Gereifat area, Red Sea coastal zone, Egypt. Egyptian Journal of Geology, 37(2): 307-333.

El-Hinnawi E, Abayazeed SD, and Khalil AS (2021). Spheroidal weathering of basalt from Gebel Qatrani, Fayum Depression, Egypt. Bulletin of the National Research Centre, 45: 1. https://doi.org/10.1186/s42269-020-00453-2

Eswaran H (1979). The alteration of plagioclases and augites under differing pedo-environmental conditions. Journal of Soil Science, 30(3): 547-555. https://doi.org/10.1111/j.1365-2389.1979.tb01008.x

Farmer VC, Russell JD, McHardy WJ, Newman ACD, Ahlrichs JL, and Rimsaite JYH (1971). Evidence for loss of protons and octahedral iron from oxidized biotites and vermiculites. Mineralogical Magazine, 38(294): 121-137. https://doi.org/10.1180/minmag.1971.038.294.01

Germann K, Schwarz T, and Wipki M (1994). Mineral deposit formation in Phanerozoic sedimentary basins of north-east Africa: The contribution of weathering. Geologische Rundschau, 83: 787-798. https://doi.org/10.1007/BF00251076

Grandstaff DT (1977). Some kinetics of bronzite orthopyroxene dissolution. Geochimica et Cosmochimica Acta, 41(8): 1097-1103. https://doi.org/10.1016/0016-7037(77)90104-1

Hampl FJ, Schiperski F, Schwerdhelm C, Stroncik N, Bryce C, von Blanckenburg F, and Neumann T (2023). Feedbacks between the formation of secondary minerals and the infiltration of fluids into the regolith of granitic rocks in different climatic zones (Chilean Coastal Cordillera). Earth Surface Dynamics, 11(3): 511-528. https://doi.org/10.5194/esurf-11-511-2023

He X, Zhou H, Wan J, Guo Y, and Zhao H (2023). The effects of rainfall on groundwater hydrogeochemistry and chemical weathering. Environmental Science and Pollution Research, 30(5): 12152-12168. https://doi.org/10.1007/s11356-022-23016-6 **PMid:36104647**

Johnson PR (2005). Proterozoic geology of western Saudi Arabia, northeastern sheet (revised, digital edition). Saudi Geological Survey Open-File Report SGS-OF-2005-2.

Johnson PR (2006). Explanatory notes to the map of Proterozoic geology of western Saudi Arabia. Saudi Geological Survey Technical Report SGS-TR-2006-4.

Kukillaya JP and Narayanan T (2014). Role of weathering of ferromagnesian minerals and surface water irrigation in evolving and modifying chemistry of groundwater in Palakkad district, Kerala, with special reference to its fluoride content. Journal of the Geological Society of India, 84: 579-589. https://doi.org/10.1007/s12594-014-0165-4

Luce RW, Bartlett RW, and Parks GA (1972). Dissolution kinetics of magnesium silicates. Geochimica et Cosmochimica Acta, 36(1): 35-50. https://doi.org/10.1016/0016-7037(72)90119-6

Mesaed AA (1995). Geological, mineralogical and geochemical studies on the ironstones and related lateritic products of Aswan region, Egypt. Ph.D. Dissertation, Cairo University, Egypt.

Meunier A and Velde B (1979). Weathering mineral facies in altered granites: The importance of local small-scale equilibria. Mineralogical Magazine, 43(326): 261-268. https://doi.org/10.1180/minmag.1979.043.326.08

Millot G (1964). Geologie des Argiles. Masson et Cie: Editeurs, Paris, France.

Murphy SF, Brantley SL, Blum AE, White AF, and Dong H (1998). Chemical weathering in a tropical watershed, Luquillo Mountains, Puerto Rico: II. Rate and mechanism of biotite weathering. Geochimica et Cosmochimica Acta, 62(2): 227-243. https://doi.org/10.1016/S0016-7037(97)00336-0

Nahon D (1987). Microgeochemical environments in lateritic weathering. In: Tardy Y and Clement Rodringer R (Eds.), Geochemistry and mineral formation in the earth surface: 141-156. Editorial CSIC-CSIC Press, Granada, Spain.

Nahon DB and Colin F (1982). Chemical weathering of orthopyroxenes under lateritic conditions. American Journal of Science, 282(8): 1232-1243. https://doi.org/10.2475/ajs.282.8.1232

Price JR and Velbel MA (2014). Rates of biotite weathering, and clay mineral transformation and neoformation, determined from watershed geochemical mass-balance methods for the Coweeta Hydrologic Laboratory, Southern Blue Ridge Mountains, North Carolina, USA. Aquatic Geochemistry, 20: 203-224. https://doi.org/10.1007/s10498-013-9190-y

Siever R and Woodford N (1979). Dissolution kinetics and the weathering of mafic minerals. Geochimica et Cosmochimica Acta, 43(5): 717-724. https://doi.org/10.1016/0016-7037(79)90255-2

Stacey JS, Stoeser DB, Greenwood WR, and Fischer LB (1984). U-Pb zircon geochronology and geological evolution of the Halaban-Al Amar region of the Eastern Arabian Shield, Kingdom of Saudi Arabia. Journal of the Geological Society, 141(6): 1043-1055. https://doi.org/10.1144/gsjgs.141.6.1043

Stoeser DB and Stacey JS (1988). Evolution, U-Pb geochronology, and isotope geology of the Pan-African Nabitah orogenic belt of the Saudi Arabian Shield. In: El-Gaby S and Greiling RO (Eds.), The Pan-African belt of Northeast Africa and adjacent areas: Tectonic evolution and economic aspects of a late Proterozoic Oregon: 227-288. Braunschweig/ Wiesbaden, Berlin, Germany.

Walker TR, Ribbe PH, and Honea RM (1967). Geochemistry of hornblende alteration in Pliocene red beds, Baja California, Mexico. Geological Society of America Bulletin, 78(8): 1055-1060. https://doi.org/10.1130/0016-7606(1967)78[1055:GOHAIP]2.0.CO;2

Xi J, Yang Y, He H, Xian H, Tan W, Li R, Zhu J, and Xu H (2024). Microstructural and compositional evolutions during transformation from biotite to berthierine: Implications for phyllosilicate alteration processes. American Mineralogist, 109(4): 656-666. https://doi.org/10.2138/am-2023-8984

Yi Z, Fu W, Zhao Q, Lu H, Fu X, Li P, Luo P, Han Z, Tan Z, and Xu C (2023). Characterization of nano-minerals and nanoparticles in supergene rare earth element mineralization related to chemical weathering of granites. American Mineralogist, 108(8): 1461-1475. https://doi.org/10.2138/am-2022-8543